

# Experimental Investigation of Optimum Beam Size for FSO Uplink

Hemani Kaushal<sup>a,\*</sup>, Georges Kaddoum<sup>b</sup>, Virander Kumar Jain<sup>c</sup>, Subrat Kar<sup>c</sup>

<sup>a</sup>*Department of Electrical, Electronics and Communication Engineering, The NorthCap University, Gurgaon, Haryana, India.*

<sup>b</sup>*Département de génie électrique, École de technologie supérieure, Montréal (QC), Canada.*

<sup>c</sup>*Electrical Engineering Department, Indian Institute of Technology Delhi, New Delhi, India.*

---

## Abstract

In this paper, the effect of transmitter beam size on the performance of free space optical (FSO) communication has been determined experimentally. Irradiance profile for varying turbulence strength is obtained using optical turbulence generating (OTG) chamber inside laboratory environment. Based on the results, an optimum beam size is investigated using the semi-analytical method. Moreover, the combined effects of atmospheric scintillation and beam wander induced pointing errors are considered in order to determine the optimum beam size that minimizes the bit error rate (BER) of the system for a fixed transmitter power and link length. The results show that the optimum beam size increases with the increase in zenith angle but has negligible effect with the increase in fade threshold level at low turbulence levels and has a marginal effect at high turbulence levels. Finally, the obtained outcome is useful for FSO system design and BER performance analysis.

**Keywords:** Turbulence, beam wander, free space optical communication, bit error rate, scintillation, OTG chamber, pointing error.

---

## 1. Introduction

Laser beam propagation through random medium such as atmosphere or underwater has been studied extensively for many years [1, 2, 3, 4, 5, 6]. This technology has several advantages over traditional radio frequency (RF) or microwave communication owing to its increased power efficiency, low mass and space requirement, higher directivity (i.e., larger antenna gain), and tariff-free extremely high bandwidth [7]. Also, FSO link provides high security due to beam confinement within a limited area and is less sensitive to electromagnetic interferences. However, various phenomena in the atmosphere such as absorption, scattering and turbulence limits the performance of FSO link. Out of these three effects, turbulence in the atmosphere can critically influence the quality of optical beam and degrade the system performance. In the case of ground-to-satellite optical communication, the major concern is due to turbulence-induced beam wander and scintillation effects[8, 9]. The beam wander induced by the turbulence causes the beam to deflect from its original line-of-sight (LOS) path leading to pointing error displacement which further induces a change in the scintillation index. This later degrades the BER performance of the system [10]. The combined effect of beam wander and intensity scintillation due to atmospheric turbulence on the BER performance of the system is significantly affected by the transmitted beam size and zenith angle. Titterton [11] was the first author to deal with scintillation and beam wander simultaneously

---

\*Corresponding author

Email address: himaniz@yahoo.com (Hemani Kaushal)

and showed that the irradiance fluctuations with combined effect were substantially larger than caused by scintillation alone. For FSO uplink, the transmitter beam size is smaller than the outer scale of turbulence and therefore, it causes the optical beam to get displaced from its on-axis position and leave the atmosphere with a significant change in direction. However, this effect is negligible during downlink from the satellite as the beam size is much larger than the turbulent eddies when it enters the Earth's atmosphere and therefore, do not displace the beam's centroid significantly [12].

Most of the previous literature have carried out a theoretical analysis of combined effect of atmospheric scintillation and pointing errors due to beam wander effect. The BER performance of ground-to-satellite FSO uplink using beam wander effect has been studied in [13]. In [14], the authors have presented a theoretical study of scintillation and beam wander analysis for ground-to-satellite uplink communication using fast-Fourier-transform beam propagation method. The spatial and temporal statistics of beam wander effect for FSO uplink has been studied analytically in [15]. In [16, 17], the authors have compared the theoretical and simulated results for analyzing the increase in scintillation due to the effect of beam wander for 10 km horizontal path propagation at high altitude. Another simulation based study on the effect of beam wander on the BER performance of FSO system using collimated and focused Gaussian beam has been carried out in [18]. A theoretical study of the influence of beam wander on ground-to-satellite FSO uplink for a collimated untracked Gaussian beam and its impact on BER system performance has been carried out in [19]. The experimental study on beam wander effect under varying atmospheric turbulence was carried out in [8]. Later in [20], the effect of spatial coherence of a Gaussian Schell-model (GSM) beam on beam wander was studied experimentally and it was demonstrated that GSM beam with low coherence experience small beam wander effect. In [21], optical spatial filter was proposed to reduce the effect beam wander caused due to turbulence in the atmosphere.

To the best of author's knowledge, the experimental investigation of optimum transmitter beam size for FSO uplink considering beam wander effect is carried out first time in this paper. Based on gamma-gamma distribution model of irradiance fluctuations, probability density function (pdf) of received irradiance is computed using a semi-analytical method by varying the temperature and wind speed inside the OTG chamber. The experimental results are then used to determine the optimum beam size that minimizes the BER performance of the system. Our work will be beneficial for system design requirements in FSO uplink communication system.

The rest of the paper is organized as follows: Section 2 describes the channel model and the effect of beam wander on ground-to-satellite FSO uplink. Experimental description and characterization of atmospheric turbulence is discussed in Section 3. Finally, the experimental results and conclusions are presented in Sections 4 and 5, respectively.

## 2. Atmospheric Turbulence and Beam Wander Effect

For ground-to-satellite FSO communication, the laser beam has to pass through random inhomogeneities in the atmosphere arising due to refractive index fluctuations. These fluctuations are described by a parameter called 'refractive index structure parameter'  $C_n^2(h)$  which gives the strength of turbulence in the atmosphere as a function of height above the ground. It is the most critical parameter that can be obtained by measuring temperature ( $T$ ), pressure ( $P$ ), wind speed ( $V$ ) and temperature

spatial fluctuations ( $\Delta T$ ) along the propagation path and is given as [22]

$$C_n^2 = \left[ 79 \times 10^{-6} \frac{P}{T^2} \right]^2 C_T^2, \quad (1)$$

where  $C_T^2$  is the temperature structure parameter which is determined by taking the measurements of mean square temperature between two points separated by a certain distance along the propagation path (in  $\text{deg}^2/\text{m}^2/3$ ) and is expressed as

$$C_T^2 = \langle \Delta T^2 \rangle r^{-1/3}, \quad (2)$$

where  $\Delta T = T_1 - T_2$  ( $T_1$  and  $T_2$  are the temperatures of two arbitrary point separated by a distance  $r$ ) and the angle bracket  $\langle \rangle$  denotes an ensemble average. The profile model of  $C_n^2$  describes the variation in structure parameter as a function of altitude  $h$ . Several day time and night time profile models are used for FSO communication [7]. One of the most popular empirical model is Hufnagel-Valley Boundary (HVB) model described by

$$\begin{aligned} C_n^2(h) = & 0.00594 \left[ \left( \frac{V}{27} \right)^2 (10^{-5}h)^{10} \exp(-h/1000) \right. \\ & + 2.7 \times 10^{-16} \exp\left(-\frac{h}{1500}\right) \\ & \left. + A \exp\left(-\frac{h}{100}\right) \right] m^{-2/3}, \end{aligned} \quad (3)$$

where  $V$  is the RMS wind speed in m/s and  $A$  is the value of refractive index structure parameter at the ground i.e.,  $C_n^2(0)$ . The presence of turbulence in the atmosphere will lead to the formation of eddies of different refractive indices and various sizes. Depending on the size of turbulent eddies and transmitter beam size, three types of atmospheric turbulence effects can be identified: beam wander, beam scintillation and beam spreading. For FSO uplink, the beam size is smaller than the turbulent eddies present in the atmospheric propagation path and therefore, the beam's instantaneous point of maximum irradiance, known as "hot spot" gets displaced from its on-axis position. This leads to significant change in the direction of the beam resulting in beam wander effect which is characterized statistically by the variance of beam wander displacement  $\langle r_c^2 \rangle$  and expressed as [16]

$$\langle r_c^2 \rangle = 0.54 (H - h_0)^2 \sec^2(\theta) \left( \frac{\lambda}{2W_0} \right)^2 \left( \frac{2W_0}{r_0} \right)^{5/3}, \quad (4)$$

where  $\theta$  is the zenith angle,  $\lambda$  is the operating wavelength,  $W_0$  is the transmitter beam size,  $H$  and  $h_0$  are the altitude of satellite and transmitter, respectively. For ground based transmitter,  $h_0 = 0$  and satellite altitude  $H = h_0 + L \cos(\theta)$ , where  $L$  is propagation length. The other parameter  $r_0$  is the atmospheric coherence length (or Fried parameter) defined by

$$r_0 = \left[ 0.423 k^2 \sec(\theta) \int_{h_0}^H C_n^2(h) dh \right]^{-3/5}, \quad (5)$$

where  $k = 2\pi/\lambda$  is the optical wave number. The beam wander effect will lead to effective pointing error of the beam  $\sigma_{pe}$  given as

$$\sigma_{pe}^2 = \langle r_c^2 \rangle \left[ 1 - \left( \frac{C_r^2 W_0^2 / r_0^2}{1 + C_r^2 W_0^2 / r_0^2} \right)^{1/6} \right]. \quad (6)$$

In the above equation, the parameter  $C_r$  is a scaling constant typically in the range from 1 to  $2\pi$ . Fig.1 shows the FSO uplink propagation model for Gaussian beam illustrating the transmitter beam size  $W_0$ , spot size  $W(L)$ , mean transmit intensity  $I(r, 0)$ , mean received intensity  $I(r, L)$  and angular pointing error  $\alpha_r$ . Beam wander induced pointing error will further increase the scintillation index whose value

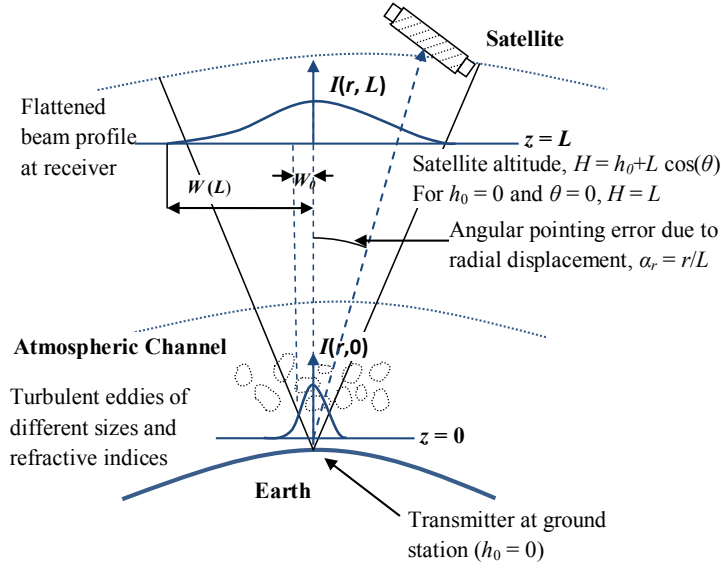


Figure 1: Beam transmission propagation model for ground-to-satellite FSO uplink.

will be different from that predicted by conventional Rytov theory[19]. According to first-order Rytov theory, the scintillation index  $\sigma_I^2$  is expressed as sum of longitudinal  $\sigma_{I,l}^2(L)$  and radial components  $\sigma_{I,r}^2(r, L)$ . However, when considering beam wander effect for FSO uplink, the increase in  $\sigma_{I,l}^2(L)$  should be considered as the effect of beam wander may increase the long-term beam profile near the bore-sight and results in a slightly flattened beam. Therefore, for FSO uplink, the longitudinal scintillation index consists of two components i.e., scintillation produced by beam wander effect and scintillation produced due to longitudinal displacement (i.e., due to intensity fluctuations of the beam not subject to beam wander effect ) which is expressed as

$$\sigma_{I,l}^2(L) = 5.95 (H - h_0)^2 \sec^2(\theta) \left( \frac{2W_0}{r_0} \right)^{5/3} \left( \frac{\alpha_{pe}}{W} \right)^2 + \sigma_{R'}^2. \quad (7)$$

In the above equation,  $\alpha_{pe} = \sigma_{pe}/L$  is the angular pointing error due to beam wander and  $\sigma_{R'}^2$  is the Rytov variance of the Gaussian beam without considering beam wander effect which is given as

$$\sigma_{R'}^2 = 8.70 \mu_1 k^{7/6} (H - h_0)^{5/6} \sec^{11/6}(\theta), \quad (8)$$

where

$$\mu_1 = \operatorname{Re} \int_{h_0}^H C_n^2(h) \left\{ (\xi)^{5/6} [\Lambda \xi + i(1 + L\xi/F)]^{5/6} - \Lambda^{5/6} \xi^{5/3} \right\} dh. \quad (9)$$

Here,  $\Lambda = 2L/kW^2$ ,  $\xi = h - h_0/H - h_0$ ,  $W$  and  $F$  are the beam spot size and radius of curvature, respectively as viewed in the receiver plane. Similarly, the radial component of scintillation is given as

$$\sigma_{I,r}^2(r, L) = 5.95 (H - h_0)^2 \sec^2(\theta) \left( \frac{2W_0}{r_0} \right)^{5/3} \times \left( \frac{\alpha_r - \alpha_{pe}}{W} \right) U(\alpha_r - \alpha_{pe}) + \sigma_{I,l}^2(L), \quad (10)$$

where  $\alpha_r = r/L$  and  $U(x)$  is a unit step function. For small radial displacement i.e.,  $r < \sigma_{pe}$ , the scintillation index  $\sigma_{I,r}^2(r, L) = \sigma_{I,l}^2(L)$ . These expressions are later used in Section 3 to study the variation of scintillation index as a function of transmitter beam size for various turbulence strength generated inside OTG chamber.

### 3. Experimental Set-up and Turbulence Characterization

This section gives the description of the experimental setup used to generate turbulence inside laboratory environment. The setup is built in such a way so that it allows the laser beam to propagate through closed turbulent chamber where the turbulence can be controlled by varying temperature or wind speed inside the chamber. Further, in order to emulate the beam propagation through decreasing temperature profile with the increase in altitude, the laser beam is allowed to pass through a vertical column where liquid nitrogen is poured from the top to build up a negative temperature gradient inside the column. An experimental setup for FSO communication consisting of a transmitter, atmospheric channel, and a receiver is shown in Fig. 2.

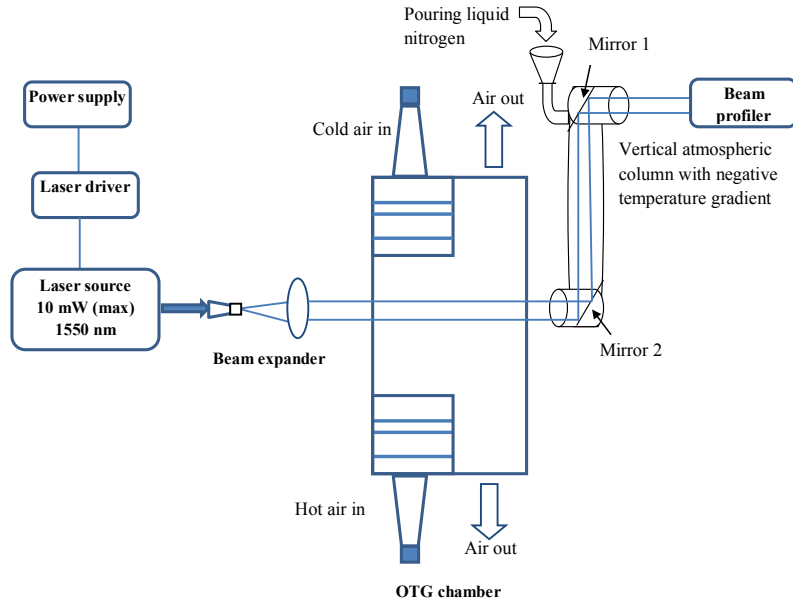


Figure 2: Experimental setup for measurement.

The transmitter used in the experiment is a laser source with maximum output power of 10 mW operating at a wavelength of 1550 nm. A beam expander is used to expand the width of transmitted beam from the laser source. This expanded beam is then passed through an atmospheric channel consisting of an OTG chamber which generates an artificial turbulence inside the laboratory environment by forced mixing of cold and hot air [8, 10]. Honeycomb filters are used to allow laminar airflow inside the mixing zone of OTG chamber. A three dimensional and top view of OTG chamber is shown in Fig. 3(a) and (b), respectively.

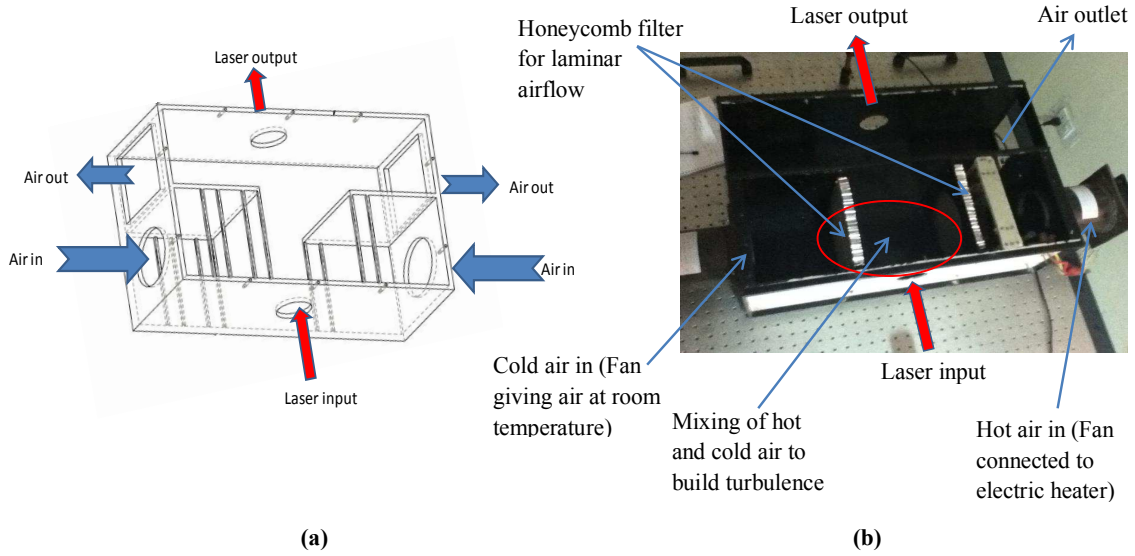


Figure 3: OTG chamber (a) Three dimensional view and (b) top view.

The dimensions of OTG chamber are 20 x 20 x 20 cm. However, the propagation length of laser beam inside the OTG chamber is increased by using a highly reflective mirror structure. Depending upon the placement of mirrors, the laser beam will travel back and forth through multiple reflections from the mirrors till it escapes from the chamber. Using this assembly, the propagation length is increased up to 5 m.

Different values of atmospheric turbulence can be generated by varying pressure, speed or temperature of the air flow inside the chamber. For this reason, the temperature inside the chamber is controlled by varying the variac connected to the heater. The air intake at one end of the channel is kept at room temperature while hot air is blown from the other side whose temperature is controlled using the electrical heater. The velocity inflow of the air is controlled by varying the rpm of the fans connected to the OTG chamber. By varying the variac connected to heater and rpm of fans, we are able to generate varying strength of turbulence inside the chamber. Laser beam propagation is kept perpendicular to the direction of the turbulent air flow. The aberrated wavefront after OTG chamber is passed through a vertical column which has a mirror arrangement inside it to allow vertical propagation of the optical beam. In order to create a negative temperature gradient as present in the atmospheric channel, we poured liquid nitrogen from the top of the vertical column. The optical beam from the vertical column is then captured by the beam profiler. Neutral density filter of transmissivity 0.3% is used before the beam profiler to avoid its saturation. The whole setup was fixed on a vibration free

table and the observations were taken in dark room environment. The complete set of parameters used in the experiment is given in Table 1.

Table 1: Parameters used in laboratory experiment

Parameters	Values
Laser power	10 mW
Operating wavelength ( $\lambda$ )	1550 nm
Variable beam expander	4 mm (max input) 45 mm (max output)
OTG chamber dimensions	20 x 20 x 20 cm
Temperature difference ( $\Delta T$ )	10 K to 90 K
Zenith angle	0 degree
Propagation length ( $L$ )	5 m
Wind speed ( $V$ )	3.5 m/s
Receiver camera type	Beam profiler
Pixel size	4.4 x 4.4 microns
Frame rate	2 frames per sec

### 3.1. Turbulence Characterization

In order to characterize the turbulence generated inside OTG chamber, experiments were carried out over several temperature ranges by varying the variac connected to the electrical heater. The wind speed was kept fixed at 3.5 m/s which is an average value of wind speed. To study the effect of turbulence-induced beam wander, fluctuations in the beam centroid were measured, firstly without OTG chamber turned on (i.e., no turbulence) and secondly with OTG chamber turned on at a fixed temperature and wind speed (i.e., with turbulence). The variance of fluctuations before OTG chamber is turned on is basically due to background noise which is subtracted from the calculations to obtain variance due to turbulence only. The experiments were carried out for six different temperature differences and corresponding values of variance were observed using beam profiler. Then using Eqs. (4) and (5), the experimental values of  $C_n^2 \cdot H$  for various temperature differences inside OTG chamber are evaluated which are shown in Table 2.

Table 2:  $C_n^2 \cdot H$  values for 1550 nm operating wavelength at wind speed of 3.5 m/s for various temperature differences

S. No.	Temperature difference $\Delta T$ (in K)	$C_n^2 \cdot H$ ( $m^{-1/3}$ )
1.	10	$5.5 \times 10^{-13}$
2.	30	$2.65 \times 10^{-12}$
3.	50	$5.92 \times 10^{-12}$
4.	70	$8.46 \times 10^{-12}$
5.	90	$5.22 \times 10^{-11}$
6.	100	$6.72 \times 10^{-11}$

## 4. Results

Following the procedure described in Section 3, the variance of beam centroid due to beam wander effect and its corresponding  $C_n^2 \cdot H$  value is observed for various temperature differences. After

characterizing the turbulence inside OTG chamber, scintillation index is determined using Eqs. 6 to 10 for a given operating wavelength,  $\lambda = 1550$  nm, zenith angle,  $\theta = 0^\circ$ , transmitter height,  $h_0 = 0$ , transmitter beam size,  $W_0$  and propagation distance,  $L = 5$  m. These values are then used to plot PDF of the received irradiance using semi-analytical method for gamma-gamma distribution model which is given as [3]

$$f_I(i) = \frac{2(\alpha\beta)^{\frac{\alpha+\beta}{2}}}{\Gamma(\alpha)\Gamma(\beta)} i^{\frac{\alpha+\beta}{2}-1} \left( \frac{i}{\langle I(r, L) \rangle} \right)^{\frac{\alpha+\beta}{2}} \times K_{\alpha-\beta} \left( 2\sqrt{\frac{\alpha\beta i}{\langle I(r, L) \rangle}} \right) \text{ for } (i > 0), \quad (11)$$

where  $\Gamma$  and  $K$  are the Gamma function and modified Bessel function of the second kind, respectively. The parameters  $\alpha$  and  $\beta$  are expressed as

$$\alpha = \left[ \exp \left\{ \frac{0.49\sigma_{R'}^2}{[1 + (2 + L/F) 0.56\sigma_{R'}^2]^{7/6}} \right\} - 1 \right]^{-1} \quad (12)$$

and

$$\beta = \left[ \exp \left\{ \frac{0.51\sigma_{R'}^2}{[1 + 0.69\sigma_{R'}^{12/5}]^{7/6}} \right\} - 1 \right]^{-1}. \quad (13)$$

$\langle I(r, L) \rangle$  is the mean intensity in the presence of turbulence and is given by

$$\langle I(r, L) \rangle = \frac{W_0^2}{W_{LT}^2} \exp \left( -\frac{2r^2}{W_{LT}^2} \right), \quad (14)$$

where  $W_{LT}$  is long term spot size which is formed by superposition of the instantaneous spots that reach the receiver and under weak fluctuations is given by

$$W_{LT} = W \sqrt{1 + (8W_0^2/r_0^2)^{5/6}}, \quad 0 \leq (8W_0^2/r_0^2) \leq 1. \quad (15)$$

Probability distribution function for received irradiance is shown in Fig. 4 for various values of temperature differences inside OTG chamber. It is observed that for a fixed transmitter beam size, increase in temperature difference (or turbulence) causes the pdf to shift towards the left till it becomes negative exponential at higher temperature difference. Further, the pdf is observed at a fixed temperature of 10 K for different values of transmitter beam size. It was observed that the intensity distribution decreases with the increase in the transmitter beam size as shown in Fig. 5. A similar trend was seen at higher values of temperature differences except that in this case, the curve shifts towards the left till the distribution becomes negative exponential. This clearly indicates the significance of transmitter beam size on the statistical characteristics of the received signal.

Fig. 6 shows the effect of transmitter beam size on the longitudinal scintillation index  $\sigma_{I,L}^2(L)$  for different values of temperature differences inside OTG chamber. It clearly indicates that there exists a particular beam size (between 2.5 mm to 4 mm) for which the beam variance due to turbulence-induced beam wander effect is minimum for given operating wavelength  $\lambda$  and propagation length  $L$ . Also, a very slight difference is observed between theoretical and experimental results for a link length of 5 m



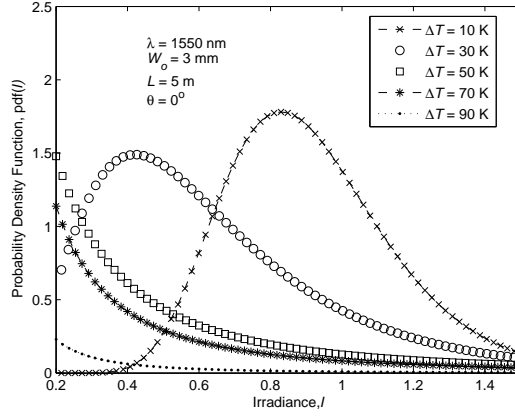


Figure 4: Probability density function of received irradiance for a fixed transmitter beam size  $W_0 = 3$  mm at various temperature differences.

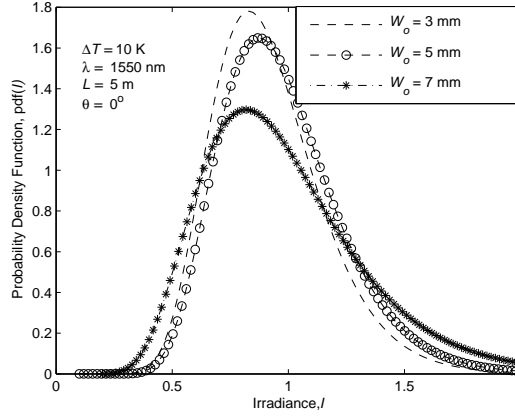


Figure 5: Variation in pdf of received irradiance with various transmitter beam size for a fixed propagation length  $L = 5$  m and temperature difference  $\Delta T = 10$  K.

operating at 1550 nm and zero zenith angle. It is to be mentioned that the trend of curve will remain same at other operating wavelengths as well, however, the dip in scintillation index may be observed at some other value of transmitter beam size. Also, in case of long link distances that cannot be emulated in laboratory controlled environment e.g., ground-to-satellite uplink communication, large scale fading effect caused due to free space path loss and beam divergence loss have to be considered.

Similarly, Fig. 7 shows the effect of radial displacement on the value of scintillation index for a given transmitter beam size. It is observed that there is very little effect on the scintillation index for a small propagation distance of 5 m. However, we see an increase in the value of scintillation index with the increase in turbulence level.

Since BER is a function of beam size and scintillation index, it is evident that there exist an optimal beam size that minimizes the BER of the system. For smaller beam size, beam wander induced pointing error increases while for larger beam size, the value of scintillation index increases. Therefore, the combined effect of beam wander induced pointing error and scintillation index will help in achieving an optimum beam size that minimizes the BER of the system. For intensity modulated system with

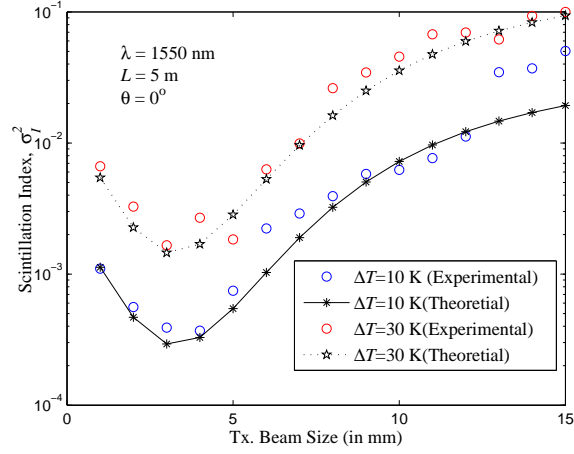


Figure 6: Longitudinal scintillation index as a function of transmitter beam size for different values of temperature differences inside OTG chamber.

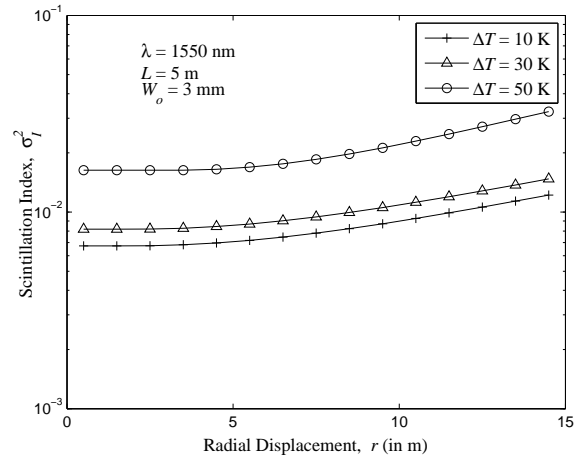


Figure 7: Scintillation index as a function of radial displacement from on-axis position for a beam size of 3 mm.

threshold  $I_{Th}$ , BER in the presence of turbulence is obtained by applying conditional averaging over the fading parameter and is given by

$$\text{BER} = \frac{1}{2} P(I \leq I_{Th}) = \frac{1}{2} \int_0^{I_{Th}} f_I(I) dI. \quad (16)$$

Usually, fade threshold parameter  $F_{Th}$  is used instead of intensity threshold which is given as

$$F_{Th} = 10 \log_{10} (\langle I(0, L) \rangle / I_{Th}). \quad (17)$$

Fig. 8 is plotted semi-analytically which shows the variation of BER with transmitter beam size for different values of temperature differences inside the OTG chamber. This figure clearly shows a dip in the value of BER around 3.7 mm to 4 mm for a fixed value of a fade threshold level at 1 dB. The variation of BER with fade threshold level for various zenith angle and temperature differences is shown

in Fig. 9. For a given transmitter beam size, an increase in fade threshold level, decreases the value of BER of the system. From Figs. 8 and 9, it is evident that BER is significantly affected by beam size, fade threshold level, and zenith angle. Also, there exist an optimum beam size for which the value of BER is minimum.

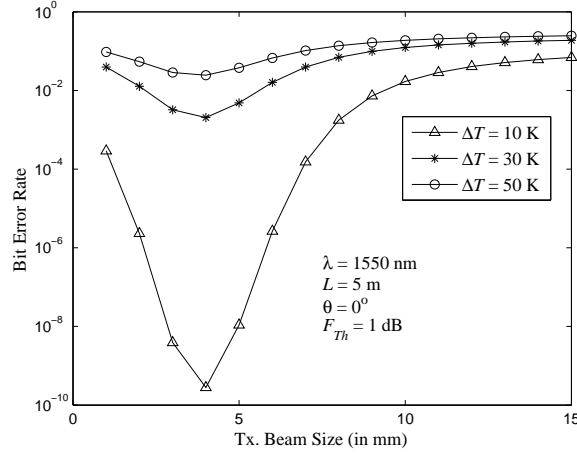


Figure 8: Variation of BER with transmitter beam size for different values of temperature difference inside OTG chamber by using semi-analytical method.

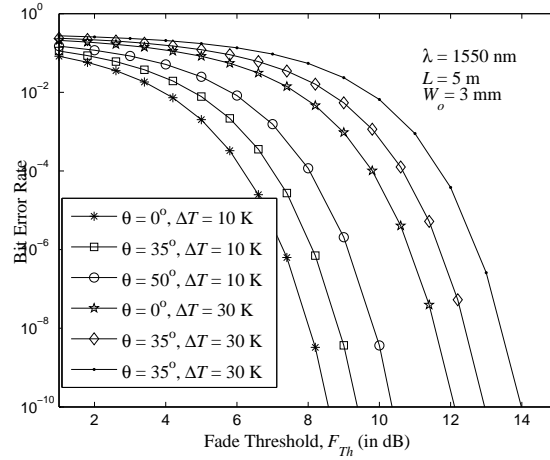


Figure 9: Variation of BER vs fade threshold level for different values of zenith angle and temperature difference inside OTG chamber by using semi-analytical method.

Figs. 10 and 11 give the variation of optimum beam size  $W_{opt}$  as a function of fade threshold level  $F_{Th}$  and zenith angle  $\theta$ , respectively for which the value of BER is minimum. It is clear from Fig. 10 that optimum beam size remains fairly constant with change in fade threshold level for low turbulence levels. However, there is a slight increase in optimum beam size for higher values of turbulence. Fig. 11 shows an increase in the value of optimum beam size with increase in zenith angle. A sharp increase in beam size is observed after zenith angle of 40 degrees.

It is clear from the results that for small propagation length  $L$  and angular displacement  $\alpha_r$  (i.e.,  $\alpha_r < \alpha_{pe}$ ), the radial component of scintillation index  $\sigma_{I,r}^2(r, L)$  vanishes and the total scintillation index

is due to longitudinal scintillation index  $\sigma_{I,l}^2(L)$  only. Since longitudinal scintillation index  $\sigma_{I,l}^2(L)$  is a function of induced pointing error due to beam wander, it gives a range of transmitter beam size for which scintillation index and correspondingly BER value is minimum for given operating wavelength, fade threshold, and propagation length. It is observed that BER is a decreasing function of a fade threshold  $F_{Th}$  whereas for a fixed  $F_{Th}$ , there exist an optimal beam size for which BER is minimum. These results are significant in the case of FSO uplink as the transmitter beam size is much smaller than the turbulent eddies near the transmitter.

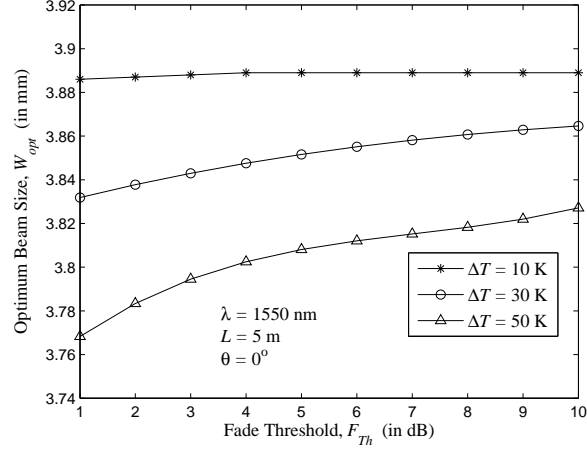


Figure 10: Variation of optimum beam size with fade threshold level for different values of temperature difference inside OTG chamber.

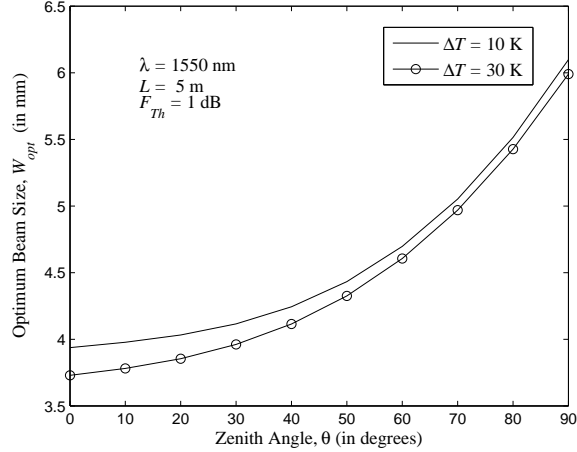


Figure 11: Variation of optimum beam size with zenith angle for different values of temperature difference inside OTG chamber.

## 5. Conclusions

In this paper, the effect of turbulence-induced beam wander variance is investigated experimentally using OTG chamber. Turbulence characterization inside OTG chamber is carried out and the results

are then used to analyze the combined effect of beam wander and scintillation for FSO uplink communication. It is shown that there exist an optimum beam size for which the value of BER is minimum for given operating wavelength, transmitter power, and link length. The optimum beam size changes its value with zenith angle and remains almost independent of a fade threshold level for low turbulence levels. However, a slight increase in optimum beam size is observed with a fade threshold level at higher values of atmospheric turbulence. These results will be useful while choosing system design parameters for FSO uplink communication.

## References

- [1] M. A. Khalighi and M. Uysal, "Survey on free space optical communication: A communication theory perspective," *IEEE Commun. Sur. & Tut.*, vol. 16, no. 4, pp. 2231–2258, 2014.
- [2] V. W. S. Chan, "Free-space optical communications," *J. Lightwave Tech.*, vol. 24, no. 12, pp. 4750–4762, 2006.
- [3] L. Yang, X. Gao, and M. S. Alouini, "Performance analysis of free-space optical communication systems with multiuser diversity over atmospheric turbulence channels," *J. IEEE Photonics*, vol. 6, no. 2, 2014.
- [4] A. K. Majumdar, "Free-space laser communication performance in the atmospheric channel," *J. Opt. Fiber Commun.*, vol. 2, no. 4, pp. 345–396, 2005.
- [5] H. Kaushal and G. Kaddoum, "Underwater optical wireless communication," *IEEE Access*, vol. 4, pp. 1518–1547, 2016.
- [6] J. A. Simpson, B. L. Hughes, and J. F. Muth, "Smart transmitters and receivers for underwater free-space optical communication," *J. IEEE Sel. Areas in Comm.*, vol. 30, no. 5, pp. 964–974, 2012.
- [7] H. Kaushal and G. Kaddoum, "Optical communication in space: Challenges and mitigation techniques," *IEEE Commun. Sur. & Tut.*, no. 99, 2016.
- [8] H. Kaushal, V. Kumar, A. Dutta, H. Aennam, V. K. Jain, S. Kar, and J. Joseph, "Experimental study on beam wander under varying atmospheric turbulence conditions," *J. IEEE Photonics Lett.*, vol. 23, no. 22, pp. 1691–1693, 2011.
- [9] J. Ma, Y. Jiang, L. Tan, S. Yu, , and W. Du, "Influence of beam wander on bit-error rate in a ground-to-satellite laser uplink communication system," *Opt. Lett.*, vol. 33, no. 22, pp. 2611–2613, 2008.
- [10] A. Viswanath, H. Kaushal, V. K. Jain, and S. Kar, "Evaluation of performance of ground to satellite free space optical link under turbulence conditions for different intensity modulation schemes," *Proc. SPIE, Free-Space Laser Communi. and Atmospheric Prop. XXVI*, vol. 8971, 2014.
- [11] P. J. Titterton, "Power reduction and fluctuations caused by narrow laser beam motion in the far field," *Appl. Opt.*, vol. 12, pp. 423–425, 1973.
- [12] C. Zhuo-li and Y. Juan-juan, "Impact of pointing errors on performance of a ground-to-satellite laser uplink communication system based on M-ary pulse position modulation," *Elsevier Science Direct*, vol. 16, pp. 20–39, 2009.

- [13] H. T. Yura and W. G. McKinley, "Optical scintillation statistics for IR ground-to-space laser communication systems," *Appl. Opt.*, vol. 22, no. 21, pp. 3353–3358, 1983.
- [14] F. Dios, J. A. Rubio, A. Rodriguez, and A. Comeron, "Scintillation and beam-wander analysis in an optical ground station-satellite uplink," *J. Appl. Opt.*, vol. 43, no. 19, pp. 3866–3873, 2004.
- [15] A. Rodriguez-Gomez, F. Dios, J. A. Antonio Rubio, and A. Comeron, "Temporal statistics of the beam-wander contribution to scintillation in ground-to-satellite optical links: an analytical approach," *Appl. Opt.*, vol. 44, no. 21, pp. 4574–4581, 2005.
- [16] L. C. Andrews, R. L. Phillips, R. J. Sasiela, and R. R. Parenti, "Strehl ratio and scintillation theory for uplink Gaussian-beam waves: beam wander effects," *J. Opt. Engg.*, vol. 45, no. 7, pp. 076001–1–076001–12, 2006.
- [17] J. Rekolons, L. C. Andrews, and R. L. Phillips, "Analysis of beam wander effects for a horizontal-path propagating Gaussian-beam wave: focused beam case," *Opt. Eng.*, vol. 46, no. 8, pp. 086002–1–086002–11, 2007.
- [18] Z. Zhao and R. Liao, "Effects of beam wander on free-space optical communications through turbulent atmosphere," *Proc. SPIE, Atmospheric Propagation VII*, vol. 7685, 2010.
- [19] H. Guo, B. Luo, Y. Ren, S. Zhao, and A. Dang, "Influence of beam wander on uplink of ground-to-satellite laser communication and optimization for transmitter beam radius," *Opt. Lett.*, vol. 35, no. 12, pp. 1977–1079, 2010.
- [20] X. Liu, F. Wang, C. Wei, and Y. Cai, "Experimental study of turbulence-induced beam wander and deformation of a partially coherent beam," *Opt. Lett.*, vol. 39, no. 11, pp. 3336–3339, 2014.
- [21] U. Darusalam, P. S. Priambodo, and E. T. Rahardjo, "Optical spatial filter to suppress beam wander and spatial noise induced by atmospheric turbulence in free-space optical communications," *J. Adv. in Opt. Tech.*, vol. 2015, pp. 1–6, 2015.
- [22] L. C. Andrews and R. L. Phillips, *Laser Beam Propagation through Random Media*. Bellingham, WA: SPIE Optical Engineering Press, 1998.